Power law of decaying homogeneous isotropic turbulence at low Reynolds number

P. Burattini,[1,*] P. Lavoie,[2] A. Agrawal,[3] L. Djenidi,[2] and R. A. Antonia[2]
[1]*Physique Statistique et Plasmas, Universite Libre de Bruxelles, B-1050 Brussels, Belgium*
[2]*Department of Mechanical Engineering, University of Newcastle, 2308 NSW, Australia*
[3]*Department of Mechanical Engineering, Indian Institute of Technology, Powai, Mumbai 400076, India*
(Received 24 November 2005; published 8 June 2006)

We focus on an estimate of the decay exponent (m) in the initial period of decay of homogeneous isotropic turbulence at low Taylor microscale Reynolds number R_λ ($\simeq 20-50$). Lattice Boltzmann simulations in a periodic box of 256^3 points are performed and compared with measurements in grid turbulence at similar R_λ. Good agreement is found between measured and calculated energy spectra. The exponent m is estimated in three different ways: from the decay of the turbulent kinetic energy, the decay of the mean energy dissipation rate, and the rate of growth of the Taylor microscale. Although all estimates are close, as prescribed by theory, that from the Taylor microscale has the largest variability. It is then suggested that the virtual origin for the decay rate be determined from the Taylor microscale, but the actual value of m be estimated from the decay rate of the kinetic energy. The dependence of m on $R_\lambda(0)$ (the value of R_λ at the beginning of the simulation) is also analyzed, using the present data as well as data from the literature. The results confirmed that m approaches 1, as $R_\lambda(0)$ increases.

DOI: 10.1103/PhysRevE.73.066304 PACS number(s): 47.27.Gs, 47.27.T−

I. INTRODUCTION

Homogeneous isotropic turbulence (HIT) has long been at the core of turbulence research. Since the seminal work of Rogallo [1], direct numerical simulations of HIT have helped to clarify, *inter alia*, the scaling properties of turbulence, the effect of the Reynolds number (R_λ), and the behavior of the velocity derivative skewness. At present, the highest-R_λ direct numerical simulations (DNS's) are performed in periodic boxes for stationary conditions, achieved through a continuous injection of energy into the largest scales. DNS's have also been performed for temporally decaying homogeneous isotropic turbulence (DHIT), where the turbulence decreases with time from an initial velocity distribution, in the absence of kinetic energy production. It has been recently suggested that some basic properties of turbulence may differ between stationary and decaying conditions, even at the same R_λ [2,3]. Further, it has been noticed [4,5] that, in pursuing ever higher values of R_λ and focusing on the smallest scales, proper resolution of the largest scales may have been overlooked. DHIT, although limited in the initial period of the decay (where a power law is established) to lower values of R_λ compared to stationary HIT, is potentially less affected by this problem. DHIT is appealing because, compared to shear flows, it avoids the complications related to a source of turbulent energy, while the properties of homogeneity and isotropy reduce sensibly the mathematical complexity of the analysis.

The experimental analog of DHIT is grid turbulence—e.g., [6,7]. In this case, the turbulence intensity decreases in the streamwise direction, as the fluid moves with a constant mean velocity away from the grid. In a frame of reference moving with the mean velocity, turbulence decays in time and is approximately homogeneous.

*FAX: +32 (0)2 650 5824. Electronic address: Paolo.Burattini@ulb.ac.be

HIT has been typically studied with the computer using finite-difference (e.g., [8]) or spectral methods (e.g., [1,9]). In this paper, we investigate DHIT by solving the lattice Boltzmann equation and we compare the results—including the kinetic energy spectrum and the velocity derivative skewness—to measurements we made in grid turbulence. The values of R_λ and the Mach number are relatively low. In the literature, there are a few simulations of HIT done with the lattice Boltzmann method (LBM) [10–12]. This method offers advantages in terms of parallelization of the algorithm for high-performance computing (e.g., [11]) and avoids the need of solving Poisson's equation for the pressure.

The main focus, here, is on temporal profiles of turbulent kinetic energy, its mean dissipation rate, and the Taylor microscale. Many studies have investigated the decay laws and similarity in DHIT [6,13–20] because these two properties allow useful generalizations in turbulence theory. In particular, Huang and Leonard [20] studied similarity and the power-law decay of box turbulence at low Reynolds number, $5 < R_\lambda < 50$, using spectral DNS's. They found that the exponent m for the kinetic energy decay $q^2 \sim t^{-m}$ (t is time) falls in the range $1.25 < m < 1.5$. They also reported on the dependence of m on R_λ. In agreement with George [18], they showed that $m \to 1$ for increasing R_λ. In this work, we propose a refined procedure to obtain m in a reliable way. The relationship between m and R_λ is of importance—for instance, in modeling small-scale turbulence. A recent work has addressed grid turbulence and its decay laws using LBM simulations [21].

II. NUMERICAL DETAILS AND INITIAL CONDITIONS

DHIT is simulated in a periodic box of 256^3 points. The Boltzmann equation is solved on a lattice for the discrete velocity distribution

$$f_\ell(\mathbf{X} + \delta_x \mathbf{e}_\ell, t + \delta_t) - f_\ell(\mathbf{X}, t) = \Omega_\ell, \quad \ell = 0, M,$$

where f_ℓ is the particle distribution function, $\mathbf{e}_\ell$ is the velocity along the ℓth direction, M is the population size, Ω_ℓ is the

TABLE I. Main parameters for the LBM simulations of box turbulence.

Case	ω	k_p	σ	$t_{\max}$	$R_\lambda(0)$	$\overline{m_q}$	$\overline{m_\lambda}$	$\overline{m_\epsilon}$	$L(0)k_{\min}$	$\eta k_{1\,\max}$	t_0
$\mathcal{A}$	1.984	9	4	9.7	170	1.39	1.34	1.39	0.33	1.0	1.08
$\mathcal{B}$	1.98	3	4	11.9	582	1.19	1.14	1.02	0.84	1.2	4.3

collision operator, $\mathbf{X}$ is the position vector, t is time, and δ_x and δ_t are the lattice space and time steps. The single relaxation time approximation [Bhatnagar-Gross-Krook (BGK) model [22]] for the collision operator has been used—i.e.,

$$\Omega_\ell = -\omega[f_\ell(\mathbf{X},t) - f_\ell^{eq}(\mathbf{X},t)],$$

where f_ℓ^{eq} is the local equilibrium distribution and ω^{-1} is the relaxation time, related to the viscosity. The lattice has unit lengths in time ($\delta_t \equiv 1$) and space ($\delta_x \equiv 1$), also denoted as lattice units (LU's). The mass density and momentum density are calculated as follows:

$$\rho = \sum_\ell f_\ell(\mathbf{X},t),$$

$$\rho\mathbf{u} = \sum_\ell f_\ell(\mathbf{X},t)\mathbf{e}_\ell,$$

where $\mathbf{u}=(u_1,u_2,u_3)$. The kinematic viscosity is

$$\nu = \left(\frac{2}{\omega} - 1\right)\frac{1}{6},$$

and the initial density is set to 0.3 (hereafter, dimensional quantities are expressed in LU's). In this work, a cubic lattice with 15 links ($d3q15$ [23,24]), including 14 velocity vectors and a rest state, is used. The speed of sound for $d3q15$ is $c_s=\sqrt{3/8}$.

The mean energy dissipation rate of the macroscopic velocity fluctuation, u_i, is defined as

$$\epsilon = \frac{\nu}{2}\left\langle\left(\frac{\partial u_i}{\partial x_j} + \frac{\partial u_j}{\partial x_i}\right)^2\right\rangle \tag{1}$$

(hereafter, unless otherwise stated, repeated indices imply summation; angular brackets denote space averaging in simulations and time averaging in experiments). Assuming isotropy, Eq. (1) reduces to

$$\epsilon = 15\nu\left\langle\left(\frac{\partial u_i}{\partial x_i}\right)^2\right\rangle \tag{2}$$

(no summation here). The Taylor microscale and Taylor-microscale Reynolds number are

$$\lambda = \frac{\langle u_1^2\rangle^{1/2}}{\langle(\partial u_1/\partial x_1)^2\rangle^{1/2}},$$

$$R_\lambda = \frac{\langle u_1^2\rangle^{1/2}\lambda}{\nu},$$

while the Kolmogorov scale is $\eta=\nu^{3/4}\epsilon^{-1/4}$. Note that both λ and R_λ are defined using only the component u_1. The integral length scale is

$$L(t) = \frac{3\pi}{4}\frac{\int_0^\infty k^{-1}E(k,t)dk}{\int_0^\infty E(k,t)dk},$$

where $E(k,t)$ is the three-dimensional (3D) energy spectrum.

The initial velocity field is prescribed by assuming the following initial (i.e., $t=0$) 3D energy spectrum:

$$E(k,0) = \frac{q^2(0)}{2}\frac{1}{A}\frac{k^\sigma}{k_p^{\sigma+1}}\exp\left[-\frac{\sigma}{2}\left(\frac{k}{k_p}\right)^2\right], \tag{3}$$

where

$$q^2(t) = \langle u_i^2\rangle = 2\int_0^\infty E(k,t)dk \tag{4}$$

is twice the mean turbulent kinetic energy [8,9]. The value of q^2 is such that the Mach number is $\ll 1$—i.e.,

$$M = \frac{q}{c_s} \simeq 0.03.$$

By using the condition (4), the constant A is

$$A = \int_0^\infty \frac{k^\sigma}{k_p^{\sigma+1}}\exp\left[-\frac{\sigma}{2}\left(\frac{k}{k_p}\right)^2\right]dk = \int_0^\infty \tilde{k}^\sigma \exp\left[-\frac{\sigma}{2}\tilde{k}^2\right]d\tilde{k},$$

where $\tilde{k}=k/k_p$. The parameters σ and k_p fix the initial conditions: the value of k_p controls the location of the peak in the initial energy spectrum, while σ determines the slope of the spectrum for $k\to 0$. The lower k_p is, the higher the initial value of R_λ—and consequently the higher R_λ is during the decay. de Bruyn Kops and Riley [4] showed that if k_p is too small, such that $Lk_{\min}<0.3$, the energy is removed too quickly from the large scales. This may compromise the initial stage of the decay [5,20]. The maximum and minimum wave numbers resolved in the present simulations are $k_{1\,\max}=2\pi/2\delta_x=\pi$ and $k_{1\,\min}=2\pi/N$. The phase of the spectral components is initialized by random numbers (see [25]). This produces an initial velocity distribution which is Gaussian (e.g., the velocity derivative skewness is zero).

In the present study, we simulate two sets of initial conditions (see Table I): case $\mathcal{A}$, for $k_p=9$ and $\sigma=4$ (which is the same slope of the von Kármán spectrum—e.g., [26]) and case $\mathcal{B}$, for $k_p=3$ and $\sigma=4$. The latter achieves a larger R_λ, comparable to values in our experiment. The simulations of case $\mathcal{B}$ are comparable to those of Antonia and Orlandi [8] and Mansour and Wray [9], who used the same σ and k_p, while studying decaying box turbulence at similar resolutions (240^3 and 270^3 for [8] and 256^3 for [9]). Hereafter, length and velocity scales are made dimensionless with N

and $[q^2(0)/2]^{1/2}$, respectively, while time scales are normalized by $N/(q^2(0)/2)^{1/2}$, as in [8,9].

To obtain the initial velocity field in physical space, the inverse Fourier transform is applied to the energy spectrum (3). Although the resulting provisional field is, by construction, divergence free in wave-number space, it is not in physical space. An iterative solution of Poisson's equation results in a solenoidal velocity field (see [25]), which can be used to initialize the distribution function f_ℓ for the LBM simulations. This procedure is different from that proposed by [10], where the initial distribution functions are calculated iteratively from the inverse-transformed velocity components, but without solving Poisson's equation. If neither of the two procedures is followed, strong pressure fluctuations develop at the beginning of each simulation, eventually compromising the entire solution. A discussion regarding the initial pressure field in lattice Boltzmann simulations (of 2D turbulence) can be found in [27].

The code for the simulation has been parallelized with MPICH2 to run on a Beowulf cluster of 16 dual-CPU PC's.

III. EXPERIMENTAL DETAILS

A low-speed wind tunnel, with a working section of 350×350 mm^2 and 2.4 m long, is used. Grids and a honeycomb section are located in the plenum chamber to homogenize and straighten the flow. A biplane square mesh grid, made up of 4.76×4.76 mm^2 square rods of solidity 0.35 and mesh size $M=24.8$ mm, is placed downstream of the primary contraction (having an area ratio of 9:1) at the beginning of the working section (which is the origin of the x axis in the streamwise direction). A secondary, axisymmetric contraction (area ratio 1.36) is placed after the grid, in order to improve the isotropy of the flow. The ratio $\langle u_1^2\rangle/\langle u_2^2\rangle$ is about 1.05, instead of 1.17 without the contraction [28] (u_1 is the component along the streamwise direction). More details on the experimental setup can be found in [29]. Measurements are made on the centerline of the working section at $x=40M$ from the grid, where the turbulence is nearly homogeneous and isotropic, according to the criteria outlined in [17]. The mean freestream velocity U is about 6 ms^{-1}.

The velocity calibration is performed *in situ*, after removing the grid. The reference velocity is measured with a Pitot-static probe connected to a differential pressure transducer (Furness FCO15, least count 0.024 mm H_2O, full range 10 mm H_2O). The streamwise velocity is measured with a single hot wire, operated with in-house constant temperature anemometer (CTA) circuits. The hot wire is etched from Pt–10% Rh to a diameter of $d_w=2.5$ μm, and the active length l_w is chosen so as to have an aspect ratio l_w/d_w of nearly 200. The CTA circuits are operated at an overheat ratio of 1.5, with a cut off frequency of approximately 15 kHz. The anemometer signals are acquired by means of a 16-bit AD board into a PC at a sampling rate of $f_s=8$ kHz, with low-pass analog filters at $f_s/2$. Taylor's hypothesis is used to convert temporal variations into spatial variations—i.e., $r_1=U/t$—and the wave number is defined as $k_1=2\pi/r_1$.

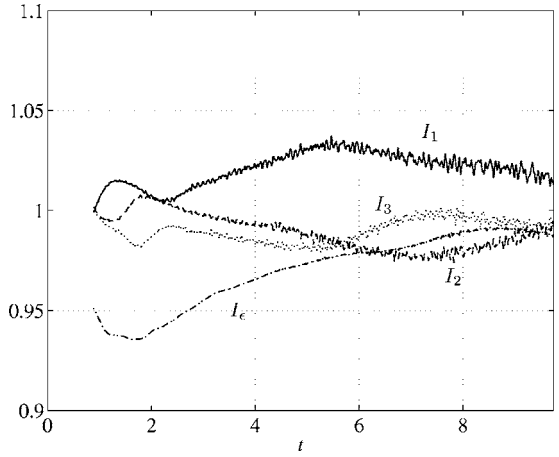

FIG. 1. Isotropy ratios for small and large scales, case $\mathcal{A}$. Solid line: $I_1=3\langle u_1^2\rangle/q^2$. Dashed line: $I_2=3\langle u_2^2\rangle/q^2$. Dotted line: $I_3=3\langle u_3^2\rangle/q^2$. Dot-dashed line: $I_\epsilon=(\epsilon_1+\epsilon_2+\epsilon_3)/3\epsilon$.

IV. RESULTS

A. Basic quantities

Isotropy at the large scales, quantified by $I_1=3\langle u_1^2\rangle/q^2$, $I_2=3\langle u_2^2\rangle/q^2$, and $I_3=3\langle u_3^2\rangle/q^2$, is shown in Fig. 1, for $\mathcal{A}$. The values are within ±3% from 1, the perfectly isotropic case. The oscillations are not systematic, and indeed they change from one simulation to another, because the initial spectrum contains a random component for the phase. The level of large-scale isotropy achieved here is superior to that in grid turbulence experiments without a secondary contraction [30–32], where I_1 can exceed 1.2.

Figure 1 shows also the small-scale isotropy quantified by $I_\epsilon=(\epsilon_1+\epsilon_2+\epsilon_3)/3\epsilon$, where the numerical subscript identifies which velocity component has been used in evaluating Eq. (2). I_ϵ is within ±2% from 1, for $t\gtrsim4$. Therefore, both large and small scales are isotropic, to a close approximation.

Figure 2 shows the temporal evolution of λ^2 for case $\mathcal{A}$.

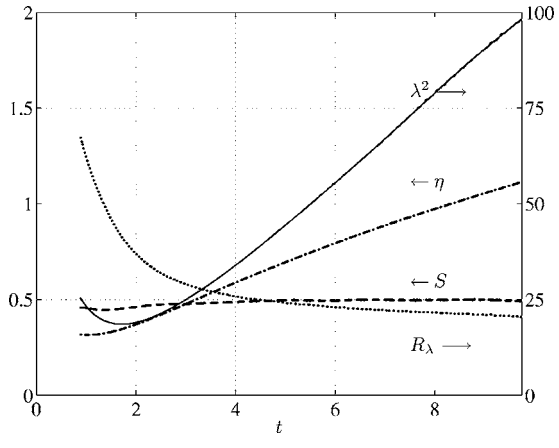

FIG. 2. Profiles of several quantities during the decay, case $\mathcal{A}$. Dotted line: R_λ. Dashed line: velocity derivative skewness. Solid line: Taylor microscale. Dot-dashed line: Kolmogorov scale. A polynomial of order 9 (almost indistinguishable from the data) is fitted to the values of λ^2.

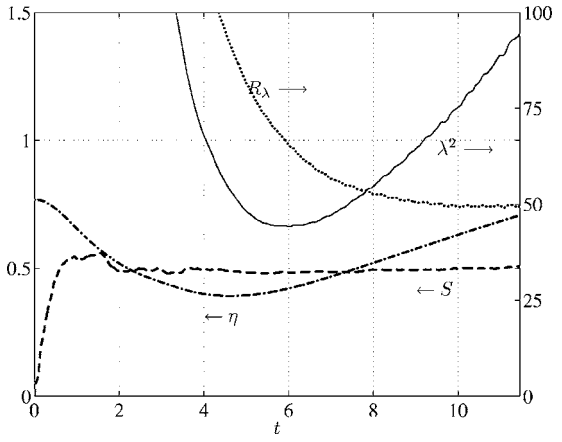

FIG. 3. Profiles of several quantities during the decay, case $\mathcal{B}$. Dotted line: R_λ. Dashed line: velocity derivative skewness. Solid line: Taylor microscale. Dot-dashed line: Kolmogorov scale.

The initial period of decay is identified with the region where λ^2 grows linearly—i.e., for $t \gtrsim 4$. The Kolmogorov scale η (same figure) increases during the initial period of decay, after having reached a minimum value of 0.3 at $t \simeq 2$.

The skewness of the velocity derivative,

$$S_i \equiv -\frac{\langle (\partial u_i/\partial x_i)^3 \rangle}{\langle (\partial u_i/\partial x_i)^2 \rangle^{3/2}}$$

(no summation implied here), has a value typically close to 0.5 in HIT and approaches zero, as $R_\lambda \to 0$. This has been shown experimentally by Tavoularis *et al.* [33], and numerically by Mansour and Wray [9] and Herring and Kerr [34]. $S=(S_1+S_2+S_3)/3$ (see Fig. 2) is close to 0.5, for $t \gtrsim 4$, in agreement with numerical [8,9] and experimental [35] data at comparable R_λ. The region where S becomes nearly constant corresponds closely to where λ^2 displays a linear growth—i.e., the initial period of decay. The development of R_λ during the simulation is also reported in Fig. 2: following an initial rapid decay, R_λ decreases more slowly for $t \gtrsim 4$.

Figure 3 reports the profiles of λ^2, η, S, and R_λ for case $\mathcal{B}$. Although the values of R_λ are larger compared to case $\mathcal{A}$, the same qualitative observations still apply.

In DHIT, there is no turbulence production so that the turbulent kinetic energy equation reduces to

$$\epsilon = -\frac{1}{2}\frac{d}{dt}q^2. \tag{5}$$

Figure 4 shows ϵ calculated from its definition [Eq. (1)] and from dq^2/dt, Eq. (5). The agreement indicates that the present simulation resolves adequately both large and small scales.

Finally, the values of the normalized energy dissipation rate

$$C_\epsilon = \frac{\epsilon L}{\langle u_1^2 \rangle^{3/2}}$$

are shown in Fig. 5. C_ϵ has been reported extensively in the literature, for both decaying and forced (i.e., stationary) box turbulence. It is widely accepted that C_ϵ achieves a constant

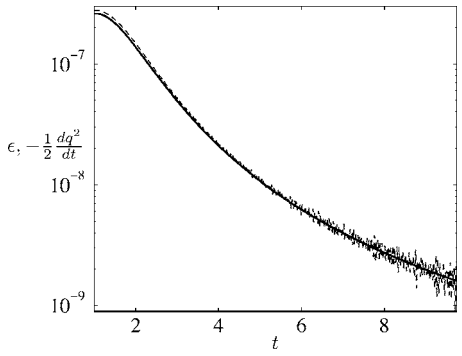

FIG. 4. Profile of the mean energy dissipation rate during the decay, case $\mathcal{A}$. Solid line: from the definition Eq. (1). Dashed line: estimated from q^2 via Eq. (5).

value near 0.5, for large R_λ, ($\gtrsim 100$) [36–38], implying that ϵ becomes independent of the viscosity, a fundamental assumption of Kolmogorov's theory [39,40]. In our simulations, R_λ is quite small so that C_ϵ is larger than 0.5: for $R_\lambda \simeq 24, C_\epsilon \simeq 1.26$ and, for $R_\lambda \simeq 44, C_\epsilon \simeq 0.71$. These values follow the same trend of previously published data (see Fig. 5 which includes data from [41]).

It is interesting to compare simulations and measurements in grid turbulence at similar values of R_λ. The numerical data refer to case $\mathcal{B}$, which achieves larger values of R_λ, close to the experimental ones. The 1D energy spectrum of u_1, $E_{11}(k_1)$, is given in Fig. 6—after normalizing k_1 by η and multiplying $E_{11}(k_1)$ by $k_1^{5/3}$. This representation would highlight the presence of the inertial range. However, the small value of R_λ ($\simeq 49$) makes such range almost nonexistent. The exponential region of the spectrum, for $k_1\eta \gtrsim 0.2$, corresponds to the dissipative range (e.g., [42]). Numerical and experimental distributions are remarkably similar. The agreement is particularly significant because no special care has been taken here, as compared to [4], in matching the initial spectrum in the simulation to that of the experiments, and also because the criterion for the large-scale resolution [4] is

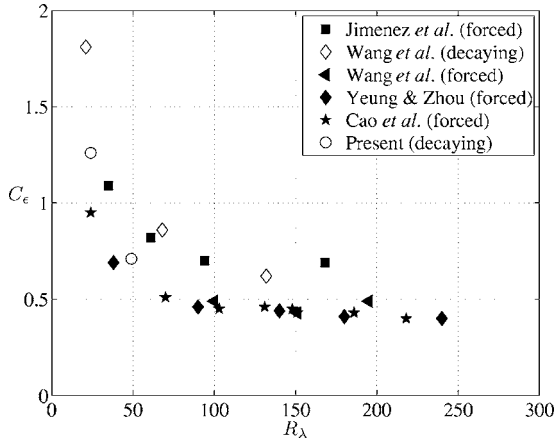

FIG. 5. Distribution of C_ϵ as a function of R_λ for different numerical simulations of decaying and forced homogeneous isotropic turbulence (adapted from [41]). (■) Jimenez *et al.* [45], (◀, ◇) Wang *et al.* [46], (♦) Yeung and Zhou [47], (★) Cao *et al.* [48], and (○) present.

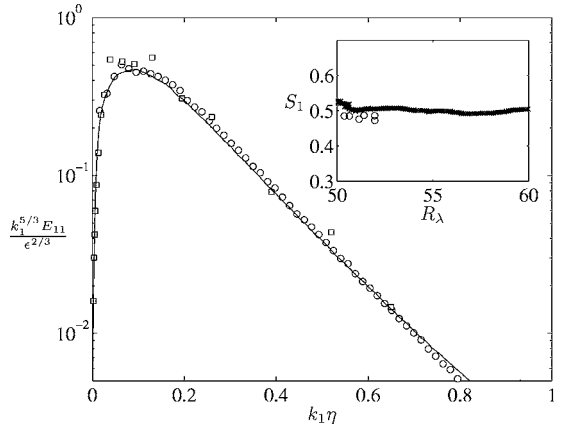

FIG. 6. Spectrum of u_1 normalized by Kolmorogov scales and compensated by $(k_1\eta)^{5/3}$. Solid line: grid turbulence, $R_\lambda=49$, present experiment (the original spectrum has been smoothed using a moving average of 20 points). (○) box turbulence (case $\mathcal{B}$, $t=10.4$), $R_\lambda=49$; (□) grid turbulence, $R_\lambda=48.6$, from [43]. Inset: velocity derivative skewness: (×) box turbulence, (○) grid turbulence.

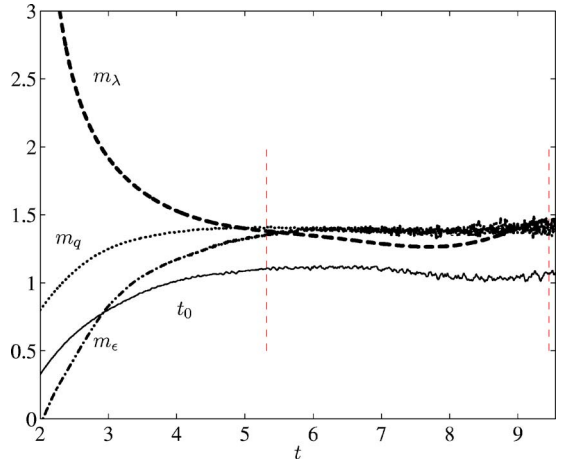

FIG. 7. (Color online) Decay exponents estimated from different quantities (case $\mathcal{A}$: see Table I. Dashed line: m_λ. Dotted line: m_q. Dot-dashed line: m_ϵ. Solid line: t_0. Vertical dashed lines indicate the time interval over which the averaged values of t_0 and m are calculated.

not strictly verified. The grid turbulence data of Comte-Bellot and Corrsin [43] at $R_\lambda \simeq 49$ are also included in the same figure, providing further support for the present results. The inset in Fig. 6 shows the profile of S_1: experimental and numerical values are again very close, at comparable R_λ.

B. Power-law decays

The decay law of the kinetic energy in DHIT has been studied extensively. Its importance is related, among other things, to closure schemes, such as the k-ϵ model [44,9]. It is *commonly accepted* that, in DHIT, the turbulent kinetic energy decays as a power law—i.e.,

$$q^2 = A(t-t_0)^{-m}, \tag{6}$$

where A is the decay constant, t_0 the virtual origin, and m the decay exponent. These three parameters are usually assumed to be constant along the decay. Batchelor and Townsend [14], who studied decaying grid turbulence, reported a value of 1 for m. Subsequently, values consistently larger than 1 have been found. At present, the range $1.15 \leqslant m \leqslant 1.45$ is deemed plausible (e.g., [26]). Equation (5) can be combined with Eq. (6) to yield

$$\epsilon = \frac{1}{2}Am(t-t_0)^{-m-1}. \tag{7}$$

From the definition of λ, it follows that

$$\lambda^2 = \frac{15\nu\langle u_1^2\rangle}{\epsilon} = \frac{10\nu}{m}(t-t_0), \tag{8}$$

which is linear in $(t-t_0)$. Therefore, differentiating λ^2 with respect to t eliminates the dependence on t_0 and yields

$$m = 10\nu/(d\lambda^2/dt). \tag{9}$$

The exponent m can thus be estimated via Eq. (6), (7), or (9), and all three should give the same result, provided Eq. (6) is valid. Nonetheless, Eq. (9) has the advantage of not containing t_0, which can be estimated afterwards from

$$t_0 = t - \frac{m}{10\nu}\lambda^2, \tag{10}$$

once m is known. [Conversely, without assuming Eq. (6), if the velocity structure functions of order 2 and 3 satisfy similarity when normalized by λ and q^2, it can be shown that q^2 decays as a power law [19].]

To investigate possible differences in the estimates of m from Eq. (6), (7), or (9), we now use different subscripts to distinguish between the different quantities on which these estimates are based—viz.,

$$q^2 = A(t-t_0)^{-m_q},$$

$$\epsilon = B(t-t_0)^{-m_\epsilon-1},$$

$$\lambda^2 = \frac{10\nu}{m_\lambda}(t-t_0).$$

Here, B is the decay constant for ϵ. The instantaneous values of m are shown as a function of t in Fig. 7. [A polynomial of order 9, almost indistinguishable from the original points (see Fig. 2), has been fitted to the values of λ^2 before taking the derivative.] From the instantaneous values, means (denoted by an overbar) are calculated, by averaging over a time interval (marked by vertical dashed lines in Figs. 7 and 8) where the distributions are nearly constant. Figure 7 shows that, for case $\mathcal{A}$, m_λ is almost constant ($\overline{m_\lambda} \simeq 1.47$) for $5.5 \leqslant t \leqslant 9.5$. In the same interval, t_0 estimated from m_λ via Eq. (10) is also nearly constant ($\overline{t_0} \simeq 1.08$). The oscillations in t_0 are due to the deviation from linearity of λ^2. With $\overline{t_0}$ determined, the instantaneous decay exponents from the kinetic energy, m_q, and from the dissipation, m_ϵ, can be estimated via Eqs. (6) and (7), Fig. 7. Although $\overline{m_\epsilon}$, $\overline{m_q}$, and $\overline{m_\lambda}$ are nearly equal (see Table I), m_λ displays larger oscillations,

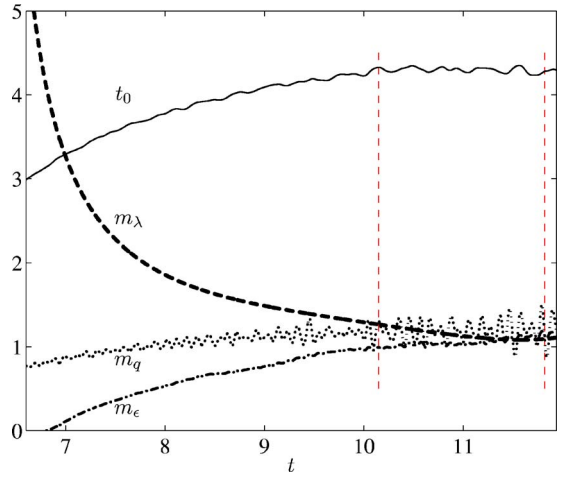

FIG. 8. (Color online) Decay exponents estimated from different quantities (case $\mathcal{B}$: see Table I). Dashed line: m_λ. Dotted line: m_q. Dot-dashed line: m_ϵ; Solid line: t_0. Vertical dashed lines indicate the time interval over which the averaged values of t_0 and m are calculated.

compared to m_ϵ and m_q. These oscillations are not systematic but change from one simulation to another: a second simulation (not shown here) with the same initial power spectrum, but different random numbers defining the phase, gave similar mean values. Case $\mathcal{B}$ at higher R_λ confirmed the accuracy of the method for evaluating m. Profiles of the instantaneous decay exponents are shown in Fig. 8, while the numerical values are listed in Table I. Compared to the lower-R_λ simulation, the initial decay is established at later times over the interval $10.1 \lesssim t \lesssim 11.8$, the origin ($\overline{t_0}=4.3$) is larger, and the decay exponent ($\overline{m_q}=1.19$) is smaller (see Table I). Similar oscillations in the values of m_λ were also reported by Huang and Leonard [20] (their Fig. 8) for values of R_λ close to the present ones. Further, as in our simulations, their distributions of q^2 seem to follow more closely a power law (their Fig. 2), in relation to those of λ^2.

The scatter in m_λ can be shown to be inherent in the definition of λ. A small error δ_ϵ, in the estimate of ϵ from the power law of q^2, is reflected in a variation Δ of the decay exponent of ϵ—viz.,

$$\delta_\epsilon = \frac{\epsilon^*}{\epsilon} = \frac{(t-t_0)^{-m_\epsilon+\Delta-1}}{(t-t_0)^{-m_\epsilon-1}} = (t-t_0)^\Delta \tag{11}$$

(the asterisk denotes the estimate affected by the error), or $m_{\epsilon^*}=m_q-\Delta$. Consequently, the Taylor microscale is also affected by Δ,

$$\lambda^{*2} = \frac{5\nu q^2}{\epsilon^*} = \frac{10\nu}{m_q}(t-t_0)^{1-\Delta}.$$

Allowing for Δ does not mean that the energy equation (5) is incorrect, but rather that Eq. (6) is only a first-order approximation. The derivative of λ^{*2} is

$$\frac{d\lambda^{*2}}{dt} = \frac{10\nu}{m_q}(1-\Delta)(t-t_0)^{-\Delta},$$

which can be used to evaluate the effect of Δ on m_λ^*—i.e.,

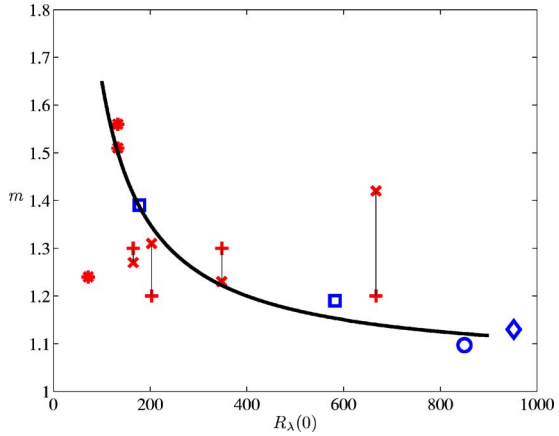

FIG. 9. (Color online) Dependence of the decay exponent (estimated from λ^2) on $R_\lambda(0)$, the Reynolds number at the beginning of the simulation. (□) present, (○) [8], (◇) [49], and (+) [20]. (×) data from [20] estimated via the decay of q^2. Vertical lines connect values of m in [20] estimated from q^2 to those estimated from λ^2 [where the two estimates coincide, an asterisk (*) appears instead]. The smooth thick line through the data, which is represented by $1.05+60/R_\lambda(0)$, is drawn as a visual aid.

$$\frac{m_\lambda^*}{m_\lambda} = \frac{d\lambda^2}{dt} \Big/ \frac{d\lambda^{*2}}{dt} = \frac{(t-t_0)^\Delta}{(1-\Delta)}. \tag{12}$$

For case $\mathcal{A}$, assuming δ_ϵ is 1.1 (i.e., an error of 10% in the estimate of ϵ from the power law of q^2) in the initial period of decay ($t=5.5$), Eq. (11) yields $\Delta=0.0641$. This is only an error of about 4.6% for m_ϵ but results in m_λ^* being 12% larger than m_λ, according to Eq. (12). Thus, even a small uncertainty in m_ϵ^* has a large effect on m_λ. Indeed, Figs. 7 and 8 show that m_λ has a larger variability, compared to m_ϵ and particularly m_q. The usual practice of determining m via q^2 in experiments is hence justified, although it should be noted that, in doing so, an initial guess for t_0 is required. This can be obtained from Eq. (10), once an initial estimate for m_λ is made.

Finally, we consider the dependence of m on $R_\lambda(0)$, the value of the Reynolds number at $t=0$. Figure 9 shows our data, as well as data from other sources, and indicates that as $R_\lambda(0)$ increases, m decreases. For some of the data in [20], there is a large difference between estimates based on λ^2 and q^2, thus raising some concern. This trend and the approach towards 1 for m at large $R_\lambda(0)$ were also documented by George [18] for grid turbulence (in [18], the values of m were plotted against R_λ in the initial period of the decay), although earlier Mohamed and LaRue [17], who compiled values of m from the literature, found that R_λ had no systematic effect on m. Arguably, in box turbulence, initial conditions can be specified more precisely than in grid turbulence so that a possible dependence on $R_\lambda(0)$ or R_λ can be discerned more easily.

V. CONCLUSIONS

Decaying homogeneous isotropic turbulence has been studied in a periodic box by solving the Boltzmann equation

on a lattice. The results are found to be consistent with simulations made with different numerical schemes and with measurements of grid turbulence. In particular, the turbulent energy spectrum and the value of the velocity derivative skewness in the initial period of decay are very close to those measured in grid turbulence.

The power laws for the decay of the turbulent kinetic energy, the decay of the mean energy dissipation rate, and the growth rate of the Taylor microscale have been analysed. Estimates of the decay exponent m obtained from these three quantities are very close, as required by theory. However, the power law for the turbulent kinetic energy is established first and displays smaller oscillations, compared to the mean energy dissipation rate and the Taylor microscale λ. The error propagation associated with the definition of λ explains the larger uncertainty in m_λ. The present data, together with other values available in the literature, suggest that m decreases towards 1, as $R_\lambda(0)$ increases.

ACKNOWLEDGMENT

The support of the Australian Research Council is acknowledged.

[1] R. S. Rogallo (unpublished).
[2] D. Fukayama, T. Oyamada, T. Nakano, T. Gotoh, and K. Yamamoto, J. Phys. Soc. Jpn. **69**, 701 (2000).
[3] R. A. Antonia and P. Burattini, J. Fluid Mech. **550**, 175 (2006).
[4] S. M. de Bruyn Kops and J. J. Riley, Phys. Fluids **10**, 2125 (1998).
[5] H. Wang and W. K. George, J. Fluid Mech. **459**, 429 (2002).
[6] G. Comte-Bellot and S. Corrsin, J. Fluid Mech. **25**, 657 (1966).
[7] P. Lavoie, P. Burattini, L. Djenidi, and R. A. Antonia, Exp. Fluids **39**, 865 (2005).
[8] R. A. Antonia and P. Orlandi, J. Fluid Mech. **505**, 123 (2004).
[9] N. N. Mansour and A. A. Wray, Phys. Fluids **6**, 808 (1994).
[10] H. Yu, S. S. Girimaji, and L.-S. Luo, Phys. Rev. E **71**, 016708 (2005).
[11] N. Satofuka and T. Nishioka, Comput. Mech. **23**, 164 (1999).
[12] H. Yu, S. S. Girimaji, and L.-S. Luo, J. Comput. Phys. **209**, 599 (2005).
[13] G. I. Taylor, Proc. R. Soc. London, Ser. A **151**, 421 (1935).
[14] G. K. Batchelor and A. A. Townsend, Philos. Trans. R. Soc. London, Ser. A **193**, 539 (1948).
[15] R. W. Stewart and A. A. Townsend, Philos. Trans. R. Soc. London, Ser. A **243** 359 (1951).
[16] G. K. Batchelor, *The Theory of Homogeneous Turbulence* (Cambridge University Press, Cambridge, England, 1953).
[17] M. S. Mohamed and J. C. LaRue, J. Fluid Mech. **219**, 195 (1990).
[18] W. K. George, Phys. Fluids A **4**, 1492 (1992).
[19] R. A. Antonia, R. J. Smalley, T. Zhou, F. Anselmet, and L. Danaila, J. Fluid Mech. **487**, 245 (2003).
[20] M.-J. Huang and A. Leonard, Phys. Fluids **6**, 3765 (1994).
[21] L. Djenidi, J. Fluid Mech. **552**, 13 (2006).
[22] P. Bhatnagar, E. Gross, and M. Krook, Phys. Rev. **94**, 511 (1954).
[23] Q. Zou and X. He, Phys. Fluids **9**, 1591 (1997).
[24] R. S. Maier, R. S. Bernard, and D. W. Grunau, Phys. Fluids **8**, 1788 (1996).
[25] P. Orlandi, *Fluid Flow Phenomena. A Numerical Toolkit* (Kluwer Academic, Dordrecht, 1999).
[26] S. B. Pope, *Turbulent Flows* (Cambridge University Press, Cambridge, England, 2000).
[27] G. Házi and C. Jiménez, Comput. Fluids **35**, 280 (2005).
[28] P. Burattini and R. A. Antonia, Exp. Fluids **38**, 80 (2005).
[29] P. Lavoie, Ph.D. thesis, University of Newcastle, 2006.
[30] T. Zhou and R. A. Antonia, J. Fluid Mech. **406**, 81 (2000).
[31] L. Mydlarski and Z. Warhaft, J. Fluid Mech. **320**, 331 (1996).
[32] H. S. Kang, S. Chester, and C. Meneveau, J. Fluid Mech. **480**, 129 (2003).
[33] S. Tavoularis, J. C. Bennett, and S. Corrsin, J. Fluid Mech. **88**, 63 (1978).
[34] J. R. Herring and R. M. Kerr, J. Fluid Mech. **118**, 205 (1982).
[35] C. W. V. Atta and R. A. Antonia, Phys. Fluids **23**, 252 (1980).
[36] T. Gotoh, D. Fukayama, and T. Nakano, Phys. Fluids **14**, 1065 (2002).
[37] Y. Kaneda, T. Ishihara, M. Yokokawa, K. Itakura, and A. Uno, Phys. Fluids **15**, L21 (2003).
[38] P. Burattini, P. Lavoie, and R. A. Antonia, Phys. Fluids **17**, 098103 (2005).
[39] A. N. Kolmogorov, Dokl. Akad. Nauk SSSR **30**, 299 (1941).
[40] K. R. Sreenivasan and R. A. Antonia, Annu. Rev. Fluid Mech. **29**, 435 (1997).
[41] K. R. Sreenivasan, Phys. Fluids **10**, 528 (1998).
[42] D. O. Martinez, S. Chen, G. D. Doolen, L.-P. Wang, and Y. Zhou, J. Plasma Phys. **57**, 195 (1997).
[43] G. Comte-Bellot and S. Corrsin, J. Fluid Mech. **48**, 273 (1971).
[44] W. K. George, H. Wang, C. Wollblad, and T. Johansson, in *Proceedings of the Australasian Fluid Mechanics Conference*, edited by B. B. Dally (Adelaide University, Adelaide, 2001), pp. 41–48.
[45] J. Jiménez, A. A. Wray, P. G. Saffman, and R. S. Rogallo, J. Fluid Mech. **255**, 65 (1993).
[46] L. P. Wang, S. Chen, J. G. Brasseur, and J. C. Wyngaard, J. Fluid Mech. **309**, 113 (1996).
[47] P. K. Yeung and Y. Zhou, Phys. Rev. E **56**, 1746 (1997).
[48] N. Cao, S. Chen, and G. D. Doolen, Phys. Fluids **11**, 2235 (1999).
[49] A. Wray (unpublished).